RESEARCH ARTICLE OPEN ACCESS

Processing-Dependent Performance of the $LiNiO_2$ Cathode in Lithium-Ion Batteries

Barbara Nascimento Nunes[1] | Ananyo Roy[1] | Aleksandr Kondrakov[1,2] | Torsten Brezesinski[1]

[1]Battery and Electrochemistry Laboratory (BELLA), Institute of Nanotechnology, Karlsruhe Institute of Technology (KIT), Karlsruhe, Germany | [2]BASF SE, Ludwigshafen, Germany

Correspondence: Barbara Nascimento Nunes (barbara.nunes@kit.edu) | Aleksandr Kondrakov (aleksandr.kondrakov@basf.com) | Torsten Brezesinski (torsten.brezesinski@kit.edu)

Received: 6 February 2026 | **Revised:** 19 March 2026 | **Accepted:** 8 April 2026

Keywords: cycling performance | Ni-rich cathode | precursor blending | rechargeable battery | surface coating

ABSTRACT

The electrochemical performance of the $LiNiO_2$ cathode is highly sensitive to minor deviations in synthesis and handling. Here, we study the effects of particle size of the precursor cathode active material (pCAM), the mixing process of pCAM and lithium source, and the impact of various atmospheres on the properties of $LiNiO_2$. For $LiNiO_2$ made from 10 μm pCAM, a performance improvement after (Nb-based) surface coating was only observed when the material was sieved in a dry room. For $LiNiO_2$ made from 4 μm pCAM, the method used to mix the hydroxide precursors (prior to calcination) proved to be decisive for the final properties, with manual grinding leading to smaller (more uniform) primary particles and enhanced stability compared to mixing with a laboratory blender. Furthermore, brief exposure of the as-prepared $LiNiO_2$ to different atmospheres resulted in some increase in initial capacity but had only a minor effect on overall performance. Notably, applying a protective surface coating did not improve cyclability, suggesting that its effectiveness depends on a variety of parameters. The results underscore the importance of carefully controlling synthesis parameters and handling conditions for $LiNiO_2$ and emphasize that detailed reporting of these factors is essential for reproducibility and further optimization.

1 | Introduction

Energy density has become one of the most critical requirements for next-generation lithium-ion batteries (LIBs), driven by the demand for longer-lasting portable electronics and more efficient electric vehicles [1, 2]. Taking this into consideration, layered Ni-rich oxides, particularly $Li(Ni_xM_{1-x})O_2$ (with $x > 0.9$ and M = Co, Al, Mn, etc.) and $LiNiO_2$ (LNO), emerge as attractive candidates for cathode active materials (CAMs) owing to their high theoretical specific capacity and favorable operating voltage range [3, 4]. However, this promise has not been realized in practice, as they are not yet commercialized due to a combination of major challenges [5–9]. For instance, these CAMs are very sensitive to the processing conditions during manufacture, with even slight deviations leading to excessive cation mixing and structural instability [10–12]. They also react strongly with moisture and CO_2, causing surface degradation and the formation of residual lithium species (Li_2CO_3, LiOH, $LiHCO_3$) [13–15]. Furthermore, their inherently poor chemo-mechanical stability leads to distinct fading during battery operation, underscoring the need for better understanding of how precursor characteristics and processing conditions influence the electrochemical behavior.

As far as synthesis is concerned, key parameters, such as the calcination temperature, lithium excess, and properties of the precursor CAM (pCAM), strongly affect the final structure and performance [6, 11, 16–18]. High calcination temperatures and increased lithium equivalents can lead to better crystallinity, broader size distribution, and lower lithium/nickel mixing (Ni_{Li} formation) [6, 16, 19]. The cyclability of the LNO cathode is also determined by the CAM|electrolyte interface, which is related to the surface area of the primary/secondary particles and can lead to

variations in first-cycle capacity loss, cycling stability, and impedance growth [6]. Aside from that, the electrochemical behavior of Ni-rich cathodes is strongly influenced by the storage conditions and post-treatment [9, 13, 20]. In this regard, washing of as-prepared LNO, for example, is required when lithium excess is used in the synthesis, as this helps remove residual surface species and increase the accessible surface area (by opening pores), thus facilitating electrolyte percolation. However, while carbonates are largely removed by dissolution, LiOH continues to form through Li^+/H^+ exchange near the surface. Note that, depending on the temperature, subsequent drying can lead to the formation of a surface layer of NiOOH- or NiO-type, which ultimately results in a significant increase in impedance [21]. Furthermore, Ni-rich cathodes are highly sensitive to air and moisture, as mentioned previously. This not only leads to accelerated degradation but also impairs the slurry stability, triggers gas evolution, and induces the formation of HF when using hexafluorophosphate-based electrolytes [22, 23]. Despite the challenges associated with post-processing and surface degradation, we have recently shown that, with a synthesis procedure in which pCAM and lithium source are homogenized through an intermediate mixing step, it is possible to produce high-quality LNO and related CAMs without the need for lithium excess, thereby eliminating subsequent washing steps [15]. Nevertheless, these surface/interface-related issues not only influence their intrinsic electrochemical performance but also have important implications for subsequent surface modification strategies. A damaged or chemically altered surface can impair the uniformity and adhesion of protective coatings, eventually reducing their effectiveness in stabilizing the cathode and mitigating adverse side reactions that occur at the CAM|electrolyte interface. Therefore, careful control of post-processing and storage is essential to ensure that the CAM lends itself to high-quality coating, especially in the case of LNO, whose surface chemistry is difficult to control because of the intrinsically poor stability. For instance, while Nb-based protective coatings on Ni-rich CAMs are not uncommon, their direct application to LNO has hardly been described in the literature [24]. Interestingly, in our previous work, high post-treatment temperatures (700°C) proved to be detrimental to the cyclability of coated LNO, although other studies on $LiNi_{0.8}Co_{0.1}Mn_{0.1}O_2$ (NCM811) have shown increased stability after Nb-based modification and calcination at 700–800°C [25–27]. This suggests that the high surface sensitivity of LNO may impose stricter requirements on coating compatibility and processing/handling conditions.

Overall, a critical aspect of the preparation of LNO is that seemingly simple processing steps can influence the surface quality and therefore the electrochemistry. In this work, we examine the direct impact of two such factors on the resulting LNO performance, namely, (i) the method for mixing the nickel and lithium hydroxide precursors in a conventional solid-state synthesis and (ii) the exposure of the material to various atmospheres during the sieving process. Although these procedures are often treated as routine steps, they can subtly affect the CAM obtained after calcination and its behavior in cycling tests. To further probe the practical impact of these variations, selected samples were also subject to Nb-based surface coating via incipient wetness impregnation (IWI), followed by calcination at 700°C. The coating served as an additional indicator of how the processing history affects the LNO particles and their ability to undergo high-temperature post-treatment while maintaining good cyclability.

2 | Results and Discussion

In our previous work, we demonstrated that the IWI method results in a more uniform surface coverage (1 mol % Nb) compared to a dry-coating process for LNO (made from 10 µm pCAM) [24]. Then, when comparing calcination temperatures (400°C versus 700°C), the IWI-derived samples treated at 700°C (IMP700, where IMP denotes LNO modified through IWI) exhibited only 66% capacity retention after 100 cycles in LIB half-cells, which was lower than the 73% retention of bare (pristine) LNO. However, across different batches of CAM, we noticed that the capacity retention varied from 66% to 80% after coating. This was attributed to differences in the pristine LNO, which had been exposed to various atmospheres during the sieving process, either in an Ar glovebox (GB) or in a dry room (DR).

To systematically assess this effect, samples from the same batch were sieved in the DR, GB, and, as an additional check, also under ambient conditions (AC) with a relatively short exposure time (∼10 min). Afterwards, they were immediately transferred to the GB and stored there. In principle, no significant variations in electrochemical performance of the pristine LNOs were observed, as shown in **Figure S1** (Supporting Information) and Table 1, with only slightly higher initial specific discharge capacity (∼224/227 mAh g^{-1} versus 218 mAh g^{-1}) and capacity retention after 100 cycles (∼73/76% versus 70%) for the samples exposed to air (i.e., LNO-DR and LNO-AC). These relatively minor differences are likely associated with chemical modifications to the surface induced during the sieving process, consistent with the formation of lithium-containing impurities, such as Li_2CO_3. Fourier-transform infrared (FTIR) spectroscopy analysis indicated the presence of carbonates, with increased intensities for LNO-AC (see **Figure S2**, Supporting Information). It has been shown that moderate amounts of Li_2CO_3, produced under controlled conditions, are not necessarily harmful to Ni-rich cathodes, particularly when not accompanied by moisture-driven LiOH and/or $LiHCO_3$ formation [20, 28].

Recently, short-term air-induced degradation mechanisms of LNO (with 6 mol % lithium excess used in the synthesis) were investigated in detail, with particular attention paid to the role of H_2O and CO_2 [28]. While H_2O induces the formation of LiOH and severe structural degradation, CO_2 primarily produces a petal-like Li_2CO_3 layer on the free surface. During the first cycles, this layer develops into an F-rich cathode electrolyte interphase (CEI), which contributes to stabilizing the CAM|electrolyte

TABLE 1 | First-cycle specific discharge capacity at 0.05C, initial Coulomb efficiency, and capacity retention after 100 cycles at 0.5C (25°C, 3.0–4.3 V vs. Li^+/Li) achieved with the LIB half-cells shown in Figures 1 and S1 (Supporting Information). All samples refer to LNO synthesized from 10 µm pCAM.

Sample	q_{dis} / mAh g^{-1}	η / %	Retention / %
LNO-GB	218.0 ± 3.6	87.5 ± 0.1	69.6 ± 4.1
IMP-GB	219.7 ± 1.2	87.6 ± 0.1	65.2 ± 1.1
LNO-DR	223.7 ± 2.1	88.8 ± 0.1	73.4 ± 3.2
IMP-DR	228.6 ± 0.8	89.4 ± 0.1	80.5 ± 1.6
LNO-AC	226.7 ± 1.0	89.0 ± 0.3	76.1 ± 1.2
IMP-AC	220.5 ± 3.4	88.4 ± 0.1	75.9 ± 1.3

interface and therefore improves performance. In contrast, moisture leads to a thicker carbonate layer containing more LiOH and $LiHCO_3$, which inevitably accelerates near-surface degradation. Consequently, brief exposure to various atmospheres may not cause major changes to the intrinsic electrochemical response of LNO. However, due to its high sensitivity to air and moisture, apparently even short-term exposure can alter the surface chemistry to such an extent that subsequent surface coatings are impaired.

For this reason, the cyclability of (Nb-based) coated LNOs (IMP-GB, IMP-DR, and IMP-AC) was evaluated and compared in LIB half-cells. It should be noted that the coating was applied after sieving the as-prepared particles in the various atmospheres. All further sample handling was carried out in the GB. Since the materials were produced using the same synthesis route, any differences in performance can be attributed to the different surface conditions prior to coating. Figure 1 shows the long-term cycling behavior at 0.5C in the potential range from 3.0 to 4.3 V vs. Li^+/Li, together with the corresponding electrochemical metrics in Table 1. The results represent the average of three independent cells per sample, including the corresponding standard deviation (SD).

After surface coating, only IMP-DR showed an improvement over the uncoated material (~81% versus 73%), whereas IMP-AC remained similar to its counterpart (~76% for both), and IMP-GB, as reported previously, exhibited a lower capacity retention than LNO-GB (~65% versus 70%). Notably, the data for the coated LNOs revealed lower SDs compared to the respective pristine counterparts (GB and DR), which is likely reflecting a more uniform surface composition after Nb-based modification and calcination at 700°C, thereby reducing variability between cells. LNO-AC also exhibited a low SD, which may be due to the fact that, compared to LNO-DR, a thicker carbonate shell forms upon brief exposure to air. As is evident, this layer impairs the effectiveness of the subsequent coating, without noticeable improvements in electrochemical performance. Regardless, the increase in capacity retention observed for IMP-DR is consistent with previous reports on NCM811 (under similar conditions) [25], suggesting that Nb-based (high-temperature) modification may indeed contribute to improving the stability of LNO. Nevertheless, the condition of the free surface prior to coating proves to be decisive for the effectiveness of the modification.

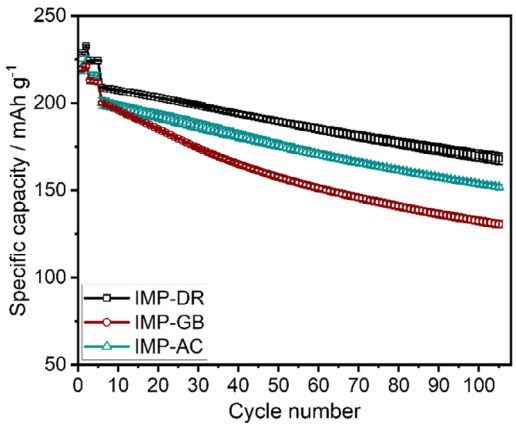

FIGURE 1 | Cycling performance of LIB half-cells with coated LNO (made from 10 µm pCAM) sieved in an Ar GB, a DR, or under AC prior to Nb-based surface modification. Specific discharge capacities are plotted against the cycle number, with error bars representing the SD. The first two cycles were performed at a rate of 0.05C, followed by three cycles at 0.1C and the subsequent ones at 0.5C (25°C, 3.0–4.3 V vs. Li^+/Li).

In our previous study, the reduced cycling stability of IMP700 (using LNO-GB) was associated with partial niobium diffusion into subsurface regions of LNO [24]. Consequently, the presence of moderate amounts of lithium residuals (LNO-DR) can limit the diffusion of Nb^{5+} into the CAM and/or alter the interfacial reactions occurring during calcination, ultimately leading to a more stable surface modification. In contrast, a thicker carbonate-based layer (LNO-AC) appears to interfere with the interactions between the niobium precursor and the LNO surface, resulting in a less effective coating.

In addition to the exposure to various atmospheres discussed, further interesting aspects were observed during the reproduction of the internally developed residual-free (RF) synthesis route [15]. In brief, in that case, the hydroxide precursor blend is first preheated and then subject to an intermediate mixing step before finally being calcined. This process enables the use of substoichiometric lithium in the synthesis, eliminating the need for washing and/or post-treatment and resulting in high-quality CAMs with record capacities. In particular, the cycling performance and stability of LNO were found to vary depending on the size of the pCAM particles and the method used for the intermediate mixing step (see **Figure S3**, Supporting Information). In fact, LNO made from 10 µm or 4 µm pCAM showed different electrochemical responses, with the mixing process playing an important role. Only the sample combining the 4 µm pCAM with manual grinding (RF-03) delivered a very high initial specific discharge capacity of $q_{dis} = (239.1 \pm 2.8)$ mAh g^{-1} at 0.05C (25°C, 2.9–4.35 V vs. Li^+/Li), in agreement with our previous study (see **Table S1**, Supporting Information). By contrast, replacing manual grinding with mixing using a laboratory blender (Kinematica) led to a reduction in q_{dis} to (220.0 ± 1.4) mAh g^{-1} and a further drop by 20–30 mAh g^{-1} in the later cycles at 0.33C. LNO made from 10 µm pCAM was less sensitive to this change in mixing method, as both samples exhibited similar behavior. This difference is likely due to the smaller discrepancy in particle size between pCAM and $LiOH{\cdot}H_2O$ (~15 µm), which reduces powder segregation during processing.

Accordingly, the effect of mixing the nickel and lithium hydroxide precursors was evaluated using a conventional solid-state synthesis route (i.e., without intermediate mixing step and using 1 mol % lithium excess). In parallel, we have investigated the effect of exposure to various atmospheres during sieving. To this end, four samples were produced, namely, KiDR and KiGB, prepared using a Kinematica blender (Ki), and MoDR and MoGB, prepared by manual grinding using a mortar and pestle (Mo). In all cases, DR and GB refer to sieving in the DR and Ar GB, respectively.

To first examine the influence of the mixing process on particle size and morphology, scanning electron microscopy (SEM) analysis was performed. In this case, only materials sieved in the GB were examined (KiGB and MoGB), as specimen preparation required brief exposure to ambient air. Overall, the different samples were similar in terms of secondary particle size and shape, see Figure 2a–f. However, higher-magnification imaging revealed that KiGB has significantly larger primary particles (grains) than MoGB. To verify whether this behavior is attributable to the 4 µm pCAM or the mixing itself, SEM images of samples made from

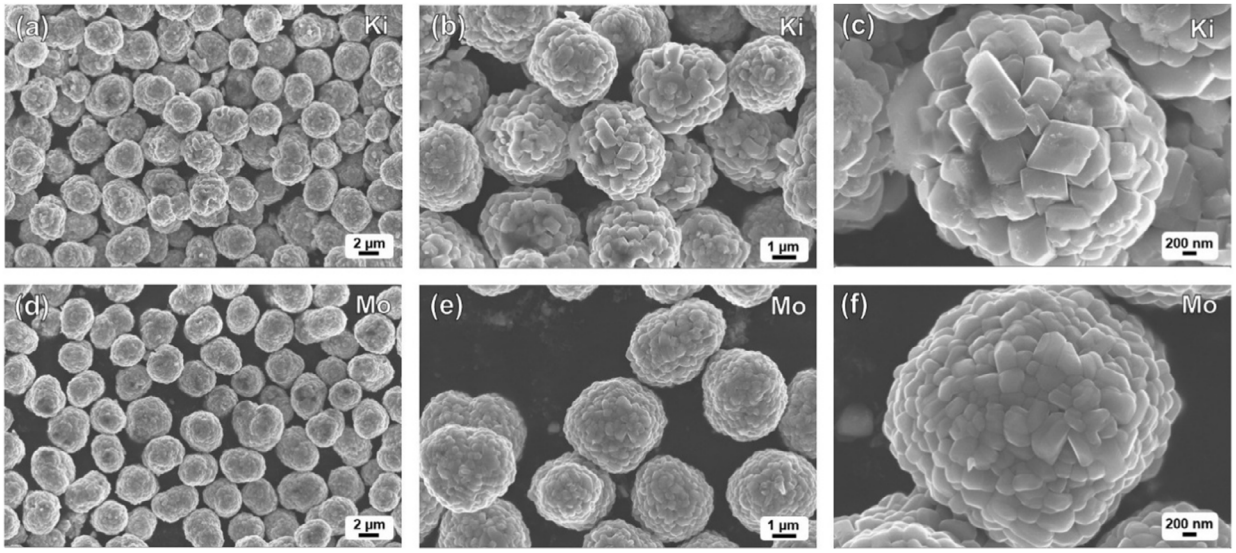

FIGURE 2 | SEM images of LNO (made from 4 µm pCAM) prepared using a Kinematica blender (Ki) or by manual grinding (Mo) and sieved in an Ar GB: (a–c) KiGB and (d–f) MoGB.

10 µm pCAM were also analyzed (see **Figure S4**, Supporting Information). Here, both KiGB and MoGB were found to exhibit comparable primary particle sizes, confirming that sensitivity to the mixing method is more pronounced when a smaller pCAM is used. Apart from that, the final LNO particles generally retained sizes close to those of the respective pCAMs. Furthermore, the KiGB samples revealed the presence of an additional material on the surface of the secondary particles, which likely originates from residual lithium.

The crystallinity of the samples synthesized using the 4 µm pCAM was investigated by X-ray diffraction (XRD), with patterns confirming the α-$NaFeO_2$-type structure within the $R\bar{3}m$ space group, as expected for LNO (see Figure 3). As can be seen, no impurity phases were detected. In addition, Rietveld analysis was performed for a more detailed evaluation of the structural parameters, with the results summarized in Table 2. While minor variations were observed between samples sieved in various atmospheres, the lattice parameters and degree of cation disorder appeared to be more strongly influenced by the mixing method used. LNOs prepared by manual grinding (MoGB and MoDR) consistently exhibited lower Ni_{Li} concentrations, as well as unit-cell volumes that were closer to the expected value for high-quality material (~101.56 Å^3) [5, 16]. By contrast, LNOs prepared using the Kinematica blender (KiGB and KiDR) showed smaller values for both the *c*-parameter and unit-cell volume, along with relatively high substitutional defect levels. In general, it has been shown that an increase in Ni_{Li} concentration leads to an expansion of the unit cell [16]. This apparent discrepancy could be related to the lower efficiency of the mixing process, in which the blender likely results in less uniform mixing due to the significant differences in particle size and mass between the nickel and lithium hydroxide precursors. However, it is important to note that the refinements were made based on laboratory XRD data; therefore, the absolute values for the defect level should only be interpreted qualitatively. Nevertheless, these trends provide evidence that the choice of mixing method in the synthesis indeed has a stronger influence on the final properties of LNO. Furthermore, the results are consistent with the SEM observations, where variations in primary particle size and surface texture clearly correlate with the mixing method used.

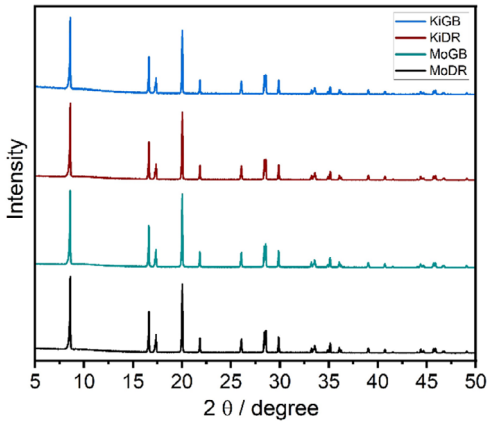

FIGURE 3 | Normalized XRD patterns of LNO (made from 4 µm pCAM) prepared using a Kinematica blender (Ki) or by manual grinding (Mo) and sieved in an Ar GB or a DR.

As shown in Figure 4a–c, the synthesis and processing variants investigated using the 4 µm pCAM led to significant differences in electrochemical performance of the respective cathodes in LIB half-cells. The first-cycle charge/discharge profiles at a rate of 0.05C were generally similar (see Figure 4a), with MoDR delivering the highest specific discharge capacity of $q_{dis} = (240.1 \pm 7.9)$ mAh g^{-1} (25°C, 3.0–4.3 V vs. Li^+/Li). This trend is confirmed by the differential capacity curves shown in Figure 4b. As can be seen, the manually ground samples (MoGB and MoDR) revealed higher peak intensities at 4.15 V during discharge (H3-H2 transition), suggesting more pronounced and better-defined redox activity in this region. Cells using KiGB or KiDR achieved similar specific discharge capacities in the initial cycle (~232 mAh g^{-1}) and showed a similar capacity retention, while MoGB and MoDR performed better, as evidenced by the long-term cycling data in Figure 4c. In fact, LNOs prepared using the Kinematica blender experienced faster fading, retaining only ~45% of their initial

TABLE 2 | Structural refinement results for LNO (made from 4 µm pCAM) prepared using a Kinematica blender (Ki) or by manual grinding (Mo) and sieved in an Ar GB or a DR.

Sample	a / Å	c / Å	c/a	V / Å^3	Ni_{Li} / %	wR	χ^2
KiGB	2.8746	14.1846	4.93	101.507	4.6	5.49	0.98
KiDR	2.8745	14.1844	4.93	101.504	3.9	5.71	1.28
MoGB	2.8754	14.1885	4.93	101.592	1.4	5.01	1.54
MoDR	2.8747	14.1886	4.94	101.548	1.9	5.90	1.17

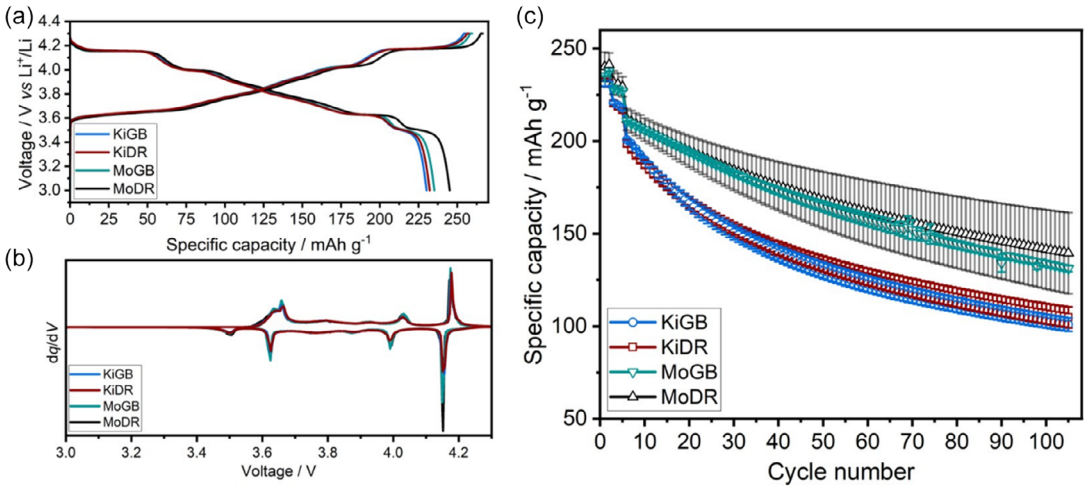

FIGURE 4 | Cycling performance of LIB half-cells with LNO (made from 4 µm pCAM) prepared using a Kinematica blender (Ki) or by manual grinding (Mo) and sieved in an Ar GB or a DR. (a) First-cycle voltage profiles, (b) corresponding differential capacity curves, and (c) specific discharge capacities as a function of cycle number, with error bars representing the SD. The first two cycles were performed at a rate of 0.05C, followed by three cycles at 0.1C and the subsequent ones at 0.5C (25°C, 3.0–4.3 V vs. Li^+/Li).

capacity at 0.5C (i.e., after rate performance testing) after 100 cycles (see Table 3). In contrast, the manually ground LNOs achieved up to 58% capacity retention. This result corroborates observations from the RF synthesis, in which the combination of 4 µm pCAM and blender (RF-01) resulted in the poorest performance, both in terms of capacity and capacity retention (see **Figure S3** and **Table S1**, Supporting Information). Aside from that, the manually ground samples appear to be more sensitive to the sieving atmosphere, with MoDR showing the overall best performance among the CAMs tested. This behavior follows a similar trend to that observed with LNO-DR and LNO-AC, which is likely related to the presence of carbonates on the particle surface. Note that the latter species can have a positive effect on initial capacity [28]. However, the SD of q_{dis} was notably higher for MoDR, which is likely due to greater heterogeneity in surface composition and/or texture caused by exposure to the DR atmosphere. Since manual grinding apparently results in fewer residual lithium on the surface of the final LNOs, MoDR appears to be more strongly affected by the exposure, ultimately leading to increased variability between cells. In contrast, MoGB delivered an initial specific discharge capacity (~235 mAh g^{-1}) that was more similar to the KiGB and KiDR samples but maintained higher capacity retention (~56%), confirming the improved stability of the manually ground samples (see Table 3).

TABLE 3 | First-cycle specific discharge capacity at 0.05C, initial Coulomb efficiency, and capacity retention after 100 cycles at 0.5C (25°C, 3.0–4.3 V vs. Li^+/Li) achieved with the LIB half-cells shown in Figure 4. All samples refer to LNO synthesized from 4 µm pCAM.

Sample	q_{dis} / mAh g^{-1}	η / %	Retention / %
KiGB	231.2 ± 1.5	90.1 ± 0.1	43.6 ± 1.6
KiDR	231.7 ± 2.3	89.7 ± 0.7	45.2 ± 2.5
MoGB	235.1 ± 0.1	90.5 ± 0.1	55.8 ± 0.7
MoDR	240.1 ± 7.9	91.2 ± 1.0	58.1 ± 9.3

Subsequently, a larger-scale synthesis (8 g versus 3 g) was carried out to enable coating studies on a single, well-defined batch of LNO, parts of which were again exposed to various atmospheres during the sieving process. In this case, manual grinding was selected as the mixing method based on the previously discussed electrochemical data. In general, MoAC* exhibited the lowest SD among the samples (see **Figure S5**, Supporting Information), consistent with observations made for LNO prepared using the 10 µm pCAM (see **Figure S1**, Supporting Information). FTIR data also indicated the presence of more surface carbonates on MoAC* (see **Figure S6**, Supporting Information). In general, compared to the LNOs produced on a smaller scale, MoGB* and MoDR* delivered slightly lower specific discharge capacities in the initial cycle (by 4–5 mAh g^{-1}), but with smaller SDs, indicating less variability between cells (see Table 4). Although MoDR* still achieved the highest discharge capacity among the three conditions, it decreased from about 240 mAh g^{-1} to 235 mAh g^{-1}.

TABLE 4 | First-cycle specific discharge capacity at 0.05C, initial Coulomb efficiency, and capacity retention after 100 cycles at 0.5C (25°C, 3.0–4.3 V vs. Li^+/Li) achieved with the LIB half-cells shown in Figures 5 and S5 (Supporting Information). All samples refer to LNO synthesized from 4 µm pCAM.

Sample	q_{dis} / mAh g^{-1}	η / %	Retention / %
MoGB*	231.5 ± 3.3	90.3 ± 1.0	65.4 ± 5.1
IMP-MoGB*	225.5 ± 0.6	90.8 ± 0.5	54.9 ± 3.5
MoDR*	235.3 ± 1.0	89.1 ± 1.9	68.6 ± 3.2
IMP-MoDR*	227.8 ± 3.4	91.1 ± 0.4	52.9 ± 2.6
MoAC*	231.7 ± 0.4	89.5 ± 0.7	72.9 ± 0.7
IMP-MoAC*	232.1 ± 1.1	91.4 ± 1.0	57.8 ± 3.8

*Samples produced from a larger batch of LNO.

This may be related to scaling factors, such as the increased amount of precursor materials during manual grinding, which could limit the mixing efficiency, as well as differences in heat distribution during calcination due to the use of a tube furnace and a larger crucible. As an additional comparison, a larger-scale synthesis was performed using the blender-based mixing process (see **Figure S5**, Supporting Information). In this case (KiGB*), a sharp decline was also observed compared to the small-scale synthesis, with the first-cycle specific discharge capacity decreasing from $q_{dis} \approx 231$ mAh g^{-1} to 201 mAh g^{-1}. These results suggest that up-scaling exacerbates the limitations of less efficient mixing in smaller pCAMs. In this regard, synthesis routes that involve additional mixing steps, such as the RF method, can be advantageous, as they improve the homogeneity of the hydroxide precursor blend and enable more effective lithiation (see **Figure S3**, Supporting Information; of note, the RF samples were produced in batches of 8 g). Regardless, future studies on homogeneity and local chemical variations using surface-sensitive techniques [e.g., X-ray photoelectron spectroscopy (XPS) or time-of-flight secondary ion mass spectrometry (ToF-SIMS)] could provide further insights.

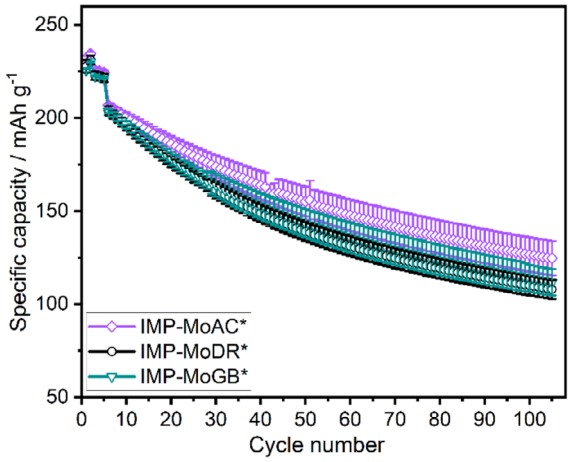

FIGURE 5 | Cycling performance of LIB half-cells with coated LNO (made from 4 µm pCAM) prepared by manual grinding (Mo) and sieved in an Ar GB, a DR, or under AC prior to Nb-based surface modification. Specific discharge capacities are plotted versus the cycle number, with error bars representing the SD. The first two cycles were performed at a rate of 0.05C, followed by three cycles at 0.1C and the subsequent ones at 0.5C (25°C, 3.0–4.3 V vs. Li^+/Li).

Finally, the three manually ground samples (MoGB*, MoDR*, and MoAC*) were subject to Nb-based surface coating via IWI, followed by thermal treatment at 700°C. In contrast to the behavior observed for LNO made from 10 µm pCAM, all three samples exhibited similar electrochemical performance (see Figure 5 and Table 4), and none of them outperformed their uncoated counterpart, indicating that, for this system, the benefits of surface modification are limited under the conditions explored in the present work. This is likely due to their larger surface area, which increases the sensitivity to surface chemistry and may require targeted optimization of the coating conditions.

3 | Conclusions

In this work, we have investigated the sensitivity of LNO to synthesis and handling conditions and have shown that even minor deviations can influence both the intrinsic properties and the outcome of subsequent surface modifications. Initially, using LNO made from 10 µm pCAM, we observed that the cycling performance of coated samples depends on the previous exposure of the pristine CAM. Exposure to various atmospheres confirmed that the Nb-based protective coating is only effective when the material is sieved in a DR.

More detailed investigations were carried out for LNO made from 4 µm pCAM, revealing that the properties depend to a large extent on the mixing method used for the precursors. Manual grinding was found to lead to smaller and more uniform primary particles (after calcination) with superior electrochemical performance over samples where pCAM and lithium source were mixed using a laboratory blender (Kinematica). When testing exposure to various atmospheres in this case, sieving in the DR slightly increased the initial capacity compared to GB conditions but had only a limited effect on the overall performance. Applying an Nb-based coating to the manually ground 4 µm samples after sieving in the different atmospheres did not result in any measurable improvements, suggesting that the effectiveness of the coating is limited, in contrast to the 10 µm case.

Overall, these results underscore the decisive influence of synthesis and handling parameters on the properties of LNO. Both the choice of mixing method for "smaller" pCAMs and short-term exposure to various atmospheres can strongly alter the surface chemistry and affect the electrochemical behavior and efficacy of subsequent surface modifications. Therefore, accurate reporting of these experimental details is essential for the reproducibility and performance optimization of LNO and related Ni-rich cathodes.

4 | Experimental

LNO Synthesis: $Ni(OH)_2$ pCAMs of diameter 4 and 10 µm were provided by BASF SE. $LiOH{\cdot}H_2O$ was added to the pCAM considering a Li:Ni molar ratio of 1.01. The solids were mixed either using a laboratory blender (Kinematica AG, MICROTRON MB 550) for 10 min in a sealed 125 mL vessel under Ar atmosphere or by manual griding in an Ar GB using an agate mortar and pestle for about 10 min. The resulting blend was transferred to

a ceramic crucible and heated for 4 h at 400°C and for another 6 h at 700°C, with a heating rate of 3°C min^{-1}, under O_2 flow (4 L h^{-1}). Sieving to 32 μm was performed either in a DR with dew point around −60°C or in an Ar GB.

Surface Coating: The IWI process was used, in which a 0.5 M ethanolic solution of $Nb(OC_2H_5)_5$ was gradually added to the LNO CAM in a ratio of 1:5 of solution to LNO (i.e., 0.4 mL for 2 g of LNO). The material was left to dry in an Ar GB, followed by heating for 2 h at 700°C under O_2 flow (7 L h^{-1}).

Characterization: Powder XRD data was collected from samples placed in 0.03 mm glass capillaries (Hilgenberg) on a STADI P (STOE) diffractometer in Debye-Scherrer geometry. Monochromatic Mo-$K_{\alpha1}$ radiation ($\lambda = 0.7093$ Å, 50 kV, 40 mA) and a MYTHEN 1K detector (DECTRIS) were used in the measurements. Rietveld analysis was performed using GSAS-II [29], allowing variations in scale factor, zero shift, and size/strain broadening parameters. A fixed background was fitted to the data as a 12-term Chebyshev polynomial. In the structural model, the unit-cell parameters, oxygen *z*-coordinate, and isotropic atomic displacement parameters for each site were refined.

SEM imaging was performed using a LEO-1530 microscope from Carl Zeiss AG, equipped with a field emission source.

FTIR data was acquired in attenuated total reflection (ATR) mode using an ALPHA FT-IR spectrometer (Bruker) in an Ar GB.

Electrochemical Testing: For electrochemical testing, a slurry was prepared first by combining the LNO with both Super C65 carbon additive (TIMCAL Ltd.) and polyvinylidene difluoride binder (Solef 5130, Solvay) in a weight ratio of 94:3:3. The slurry was cast onto Al foil of thickness 0.03 mm using a stainless-steel doctor blade on an Erichsen Coatmaster 510 (Erichsen GmbH & Co. KG) as film applicator. Subsequently, the as-prepared cathodes were dried under dynamic vacuum at 120°C overnight, calendared at 14 N mm^{-1} (Sumet Technologies GmbH & Co. KG), and cut into circular electrodes (13 mm diameter). The areal loading was about 9 mg_{LNO} cm^{-2}. Coin half-cells were assembled using a Whatman glass-fiber separator of GF/D type, LP57 electrolyte (1 M $LiPF_6$ in 3:7 by weight of ethylene carbonate and ethyl methyl carbonate), and a lithium-metal anode in an Ar GB. They were crimped at a pressure of 1.1 t. 1C was defined as 200 mA $g_{LNO}{}^{-1}$. All cycling data is averaged from two or three independent cells.

Acknowledgments

This work was supported by BASF SE. The authors are grateful to the Federal Ministry of Research, Technology and Space (BMFTR) for funding within the projects SUSTRAB (03XP0415D) and UNIKAM (03XP0484B). The authors thank Fatih Ulusoy (KIT) for SEM imaging.

Open Access funding enabled and organized by Projekt DEAL.

Conflict of Interest

The authors declare no conflicts of interest.

Data Availability Statement

The data that support the findings of this study are available from the corresponding author upon reasonable request.

References

1. A. Kwade, W. Haselrieder, R. Leithoff, A. Modlinger, F. Dietrich, and K. Droeder, "Current Status and Challenges for Automotive Battery Production Technologies," *Nature Energy* 3 (2018): 290–300.

2. D. Baek, A. Bocca, and A. Macii, "A Cost of Ownership Analysis of Batteries in All-Electric and Plug-in Hybrid Vehicles," *Energy, Ecology & Environment* 7 (2022): 604–613.

3. W. Li, E. M. Erickson, and A. Manthiram, "High-Nickel Layered Oxide Cathodes for Lithium-Based Automotive Batteries," *Nature Energy* 5 (2020): 26–34.

4. Z. Wu, C. Zhang, F. Yuan, et al., "Ni-Rich Cathode Materials for Stable High-Energy Lithium-Ion Batteries," *Nano Energy* 126 (2024): 109620.

5. M. Bianchini, M. Roca-Ayats, P. Hartmann, T. Brezesinski, and J. Janek, "There and Back Again—the Journey of $LiNiO_2$ as a Cathode Active Material," *Angewandte Chemie International Edition* 58 (2019): 10434–10458.

6. F. Riewald, P. Kurzhals, M. Bianchini, H. Sommer, J. Janek, and H. A. Gasteiger, "The $LiNiO_2$ Cathode Active Material: A Comprehensive Study of Calcination Conditions and Their Correlation with Physicochemical Properties Part II. Morphology," *Journal of the Electrochemical Society* 169 (2022): 020529.

7. L. Karger, A. Kondrakov, and T. Brezesinski, "On the Mechanistic Understanding of First-Cycle Capacity Loss in Polycrystalline and Single-Crystal Layered Ni-Rich Oxide Cathodes for Li-Ion Batteries," *ChemistryEurope* 3 (2025): e202500097.

8. L. de Biasi, A. Schiele, M. Roca-Ayats, et al., "Phase Transformation Behavior and Stability of $LiNiO_2$ Cathode Material for Li-Ion Batteries Obtained from In Situ Gas Analysis and Operando X-Ray Diffraction," *ChemSusChem* 12 (2019): 2240–2250.

9. M. Cai, W. Yang, and Z. Wu, "Modification Strategies of High-Nickel Layered Oxide Cathode for Lithium-Ion Batteries," *Batteries & Supercaps* 8 (2025): e202500095.

10. F. Liu, S. Li, C. Leung, et al., "Unveiling the Origin of Oxygen Framework Stability in Ultra-High Nickel Layered Oxide Cathodes," *Advanced Materials* 37 (2025): 2419856.

11. Y. Sun, C. Li, J. Chen, et al., "In Situ Crystal Structure Growth and Control for Enhancing Comprehensive Performance in Ultra-High Nickel-Layered Lithium Cathodes," *Angewandte Chemie International Edition* 65 (2026): e13466.

12. H. Li, A. Liu, N. Zhang, et al., "An Unavoidable Challenge for Ni-Rich Positive Electrode Materials for Lithium-Ion Batteries," *Chemistry of Materials* 31 (2019): 7574–7583.

13. W. M. Seong, Y. Kim, and A. Manthiram, "Impact of Residual Lithium on the Adoption of High-Nickel Layered Oxide Cathodes for Lithium-Ion Batteries," *Chemistry of Materials* 32 (2020): 9479–9489.

14. Z. Cui, P. Zuo, Z. Guo, C. Wang, and A. Manthiram, "Formation and Detriments of Residual Alkaline Compounds on High-Nickel Layered Oxide Cathodes," *Advanced Materials* 36 (2024): 2402420.

15. L. Karger, R. Yao, K. Seidel, et al., "Solving the Residual Lithium Problem by Substoichiometric Synthesis of Layered Ni-Rich Oxide Cathodes," *ACS Energy Letters* 9 (2024): 5573–5575.

16. P. Kurzhals, F. Riewald, M. Bianchini, H. Sommer, H. A. Gasteiger, and J. Janek, "The $LiNiO_2$ Cathode Active Material: A Comprehensive Study of Calcination Conditions and Their Correlation with Physicochemical Properties. Part I. Structural Chemistry," *Journal of the Electrochemical Society* 168 (2021): 110518.

17. J. Pan, L. Xie, Y. Wang, et al., "Reevaluating the Critical Role of Cobalt in Ultra-High Nickel Cathodes: Toward Sustainable and High-Performance Lithium-Ion Batteries," *Advanced Functional Materials* 36 (2026): e11503.

18. L. Qiu, M. Zhang, W. Hua, et al., "Unveiling Surface Reconstruction as the Primary Trigger for Capacity Loss in Ultra-High Nickel Cathodes," *Angewandte Chemie International Edition* 64 (2025): e202417278.

19. Z. Qiu, Z. Wang, and S. Yuan, "How Sintering Temperature Affects the Electrochemical Performance of Ultra-High Nickel (Ni > 0.9) Cathode Material," *Journal of Colloid and Interface Science* 656 (2024): 225–232.

20. N. V. Faenza, L. Bruce, Z. W. Lebens-Higgins, et al., "Growth of Ambient Induced Surface Impurity Species on Layered Positive Electrode Materials and Impact on Electrochemical Performance," *Journal of the Electrochemical Society* 164 (2017): A3727–A3741.

21. D. Pritzl, T. Teufl, A. T. S. Freiberg, et al., "Washing of Nickel-Rich Cathode Materials for Lithium-Ion Batteries: Towards a Mechanistic Understanding," *Journal of the Electrochemical Society* 166 (2019): A4056–A4066.

22. D. Cao, C. Tan, and Y. Chen, "Oxidative Decomposition Mechanisms of Lithium Carbonate on Carbon Substrates in Lithium Battery Chemistries," *Nature Communications* 13 (2022): 4908.

23. A. T. S. Freiberg, J. Sicklinger, S. Solchenbach, and H. A. Gasteiger, "Li_2CO_3 Decomposition in Li-Ion Batteries Induced by the Electrochemical Oxidation of the Electrolyte and of Electrolyte Impurities," *Electrochimica Acta* 346 (2020): 136271.

24. B. N. Nunes, L. Karger, R. Zhang, A. Kondrakov, and T. Brezesinski, "Enhanced Cycling Performance of the $LiNiO_2$ Cathode in Li-Ion Batteries Enabled by Nb-Based Surface Coating," *ChemSusChem* 18 (2025): e202402202.

25. F. Xin, H. Zhou, Y. Zong, et al., "What Is the Role of Nb in Nickel-Rich Layered Oxide Cathodes for Lithium-Ion Batteries?," *ACS Energy Letters* 6 (2021): 1377–1382.

26. J. H. Kim, H. Kim, W. Choi, and M.-S. Park, "Bifunctional Surface Coating of $LiNbO_3$ on High-Ni Layered Cathode Materials for Lithium-Ion Batteries," *ACS Applied Materials & Interfaces* 12 (2020): 35098–35104.

27. B. N. Nunes, W. van den Bergh, F. Strauss, A. Kondrakov, J. Janek, and T. Brezesinski, "The Role of Niobium in Layered Oxide Cathodes for Conventional Lithium-Ion and Solid-State Batteries," *Inorganic Chemistry Frontiers* 10 (2023): 7126–7145.

28. H. Yi, J. Wang, G. Luo, et al., "Decoupling Ambient Air-Induced Degradation Mechanism of $LiNiO_2$ during Short-Time Storage," *Journal of Energy Chemistry* 115 (2026): 42–53.

29. B. H. Toby and R. B. Von Dreele, "GSAS-II: The Genesis of a Modern Open-Source All Purpose Crystallography Software Package," *Journal of Applied Crystallography* 46 (2013): 544–549.

Supporting Information

Additional supporting information can be found online in the Supporting Information section.